Problem of safety in nanoparticle mass production and its solution by means of advanced scanning electron microscopy

2011 J. Phys.: Conf. Ser. 291 012014

(http://iopscience.iop.org/1742-6596/291/1/012014)

Journal of Physics: Conference Series **291** (2011) 012014 doi:10.1088/1742-6596/291/1/012014

Problem of safety in nanoparticle mass production and its solution by means of advanced scanning electron microscopy

S.K. Maksimov; K.S. Maksimov

Moscow Institute of Electronic Technology, Russia

E-mail: maksimov_sk@comtv.ru

Abstract. It is suggested possible approaches to the comprehensive solution of the problem of structural-morphological control in mass production of nanoparticles only by the use of advanced methods of scanning electron microscopy.

1. Introduction

Outgoing production control is the integral part of any technology. It must secure conformity of a controlled portion of production with its technical regulations and thereby lock in its quality and compatibility with the biosphere. Risks connected with nanodimensional particles for the life are associated with their capacity to control reactions in ambient environment [1], i.e., with their catalytic activity. Catalytic activity of solid objects is controlled by their structure and crystallographic faceting or a habit [2]. Size, structure and habit are thermodynamically interconnected in the nanoworld, and decrease of particle sizes leads to change of its equilibrium structure and habit [3, 4]. However thermodynamics determines only a direction of possible phase transitions, but their realisation is controlled by factors controlling the kinetics of nucleation and growth of particles. Technologies, which allow obtaining particles of only one single size, are impossible. Therefore particles of the same size and obtained in the same process can be of different structural-morphological characteristics and, naturally, of different catalytic properties. Environmental safety in mass production of particles can be provided only by means of revealing of fractions of particles with peculiar structural-morphological characteristics [5, 6]. The urgent need of the factional control is emphasized by such problems as the property of nanodimensional anatase particles to modify DNA [7] (the anatase is present at medicines comprising TiO_2, e.g., at the Tamsulosin, Ofloxacin, etc) or the possibility of use of nanocrystallization for increasing solubility of pharmaceutical substances [8].

A spatial resolution that makes it possible to solve problems of structural-morphological characterization of nanoparticles is provided by scanning probe microscopy (SPM), transmission electron microscopy (TEM) and scanning electron microscopy (SEM). SPM and TEM allow determining a habit of a sole object with the highest accuracy and precision [2, 9]. However massifs numbering billions of particles have to arise in the large-scale manufacturing, whereas investigations of influence of nanoparticles on the metabolism have been carried out only for subjects with small duration of a life cycle [10], and it is no way of telling: “how much a number of particles can result in irreversible consequences throughout human lifetime”. The environmental safety requires identification of fractions, a portion of which can be equal, at least, to $10^{-4} – 10^{-6}$ of total number of nanoobject of a massif and, accordingly, controlled massifs must exceed $10^6 – 10^8$ particles [2, 11].

Productivity of SPM and TEM are not sufficient for the control of massifs numbering ≥ 10^6 objects [2, 9].

SEM techniques allow, in principle, getting images of massifs of nanoobjects practically infinite by numbers. SEM images depend only from an object habit and its tilting about an electron beam direction, if conditions of an image obtaining (electron energy, beam convergence, focusing distance, etc) as well an object composition are constant [12]. Images of objects can be dividing into groups in compliance with such image characteristics as a size, shape and intensity distribution (Fig. 1).

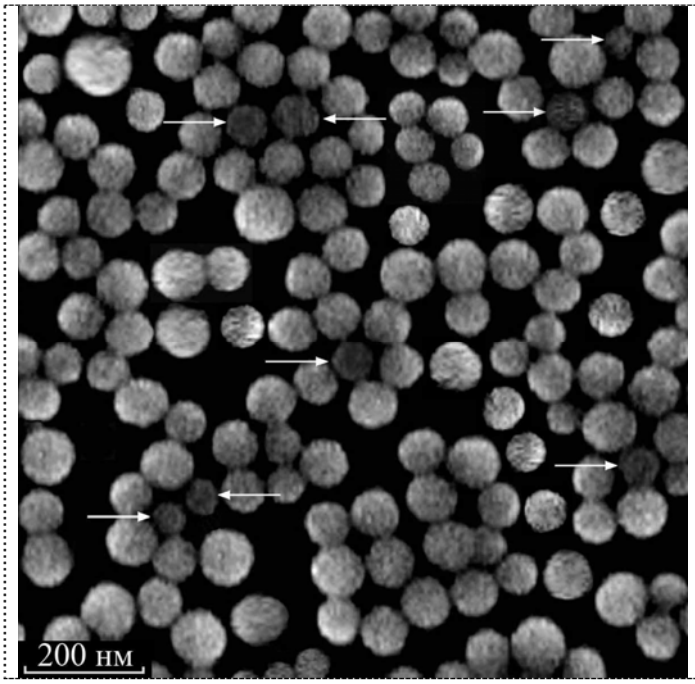

Figure 1. SEM images of SiO_x particles. Particle images differ in average intensity and contrast range. Images with anomalously lowered intensity are shown by arrows.

Images with less average intensity and contrast in Fig.1 can correspond to particles of another nature than images with more typical characteristics, and revelation of SEM images with different characteristics could be the basis for control of massifs with any quantity of nanoparticles. How-ever only a direct determination of structural-morphological characteristics particles with unusual images can assure a valid conclusion concerning their nature [13].

2. Approach to the methods of the habit determination.

SEM images arise in the course of electron beam scanning over the surface of the object and represent the sum of sequential responses generated by the object in response to inelastic scattering of electrons of an illuminating beam. The intensity profiles have the shape of curves on which points corresponding to the edges of the object cannot be determined; i.e., the sizes of the object cannot be directly measured [12]. Methods of the stereo microscopy, basing on images corresponding to different projections of object, are not valid with decreasing sizes for this reason. Technique allowing studying their habit is suggested in this paper. It can be realized with the help of secondary electrons with energy of 20 – 50 eV (this energy region provides the minimal free path of recoil electrons [13]).

When an illuminating electron beam scans the surface of a relief object in SEM, the probe becomes alternately farther and closer to the focusing plane and its sizes change; i.e., a movement provokes defocusings. Modern SEM techniques are based on illuminating electron beams with convergence angles which are equal to $\geq 3\times10^{-3}$ rad, and therefore a depth of the focus of SEM at maximal magnifications is equal to $\approx$ 0.5 μm [13]; i.e., in the majority of cases, it exceeds a height of an object, and an image is insensible to these defocusings. But if the angle of convergence reaches $\approx 10^{-1}$ rad,

the depth of the focus becomes equal to or less than 10 nm, that gives rise to noticeable defocusings even for objects with a height of ≤ 10 nm [11] (Fig. 2).

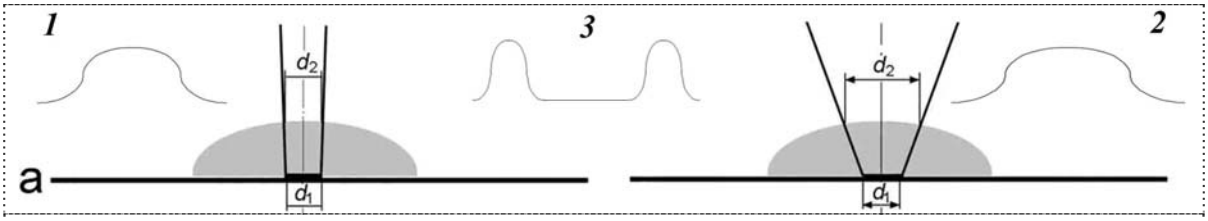

Figure 2. Diagrammatic representation of influence of the habit defocusing on BE images. ***1*** – the illuminating beam with a small angle of convergence and typical intensity profile in this case, ***2*** – the illuminating beam with a large angle of convergence and typical intensity profile in this case; ***3*** – a differential curve; "*a*" is a substrate plane; "d_1" is a size of a beam cross-sections by a substrate (focusing plane, datum plane); "d_2" is a size of a probe.

Hereinafter, 2 variants of convergences are subsequently referred to as the 1st or 2nd convergences in accordance with Fig. 1, the term "probe" applies to a cross-section of an illuminating beam by an object surface, and the term "beam-section" means the a cross-section of an illuminating beam by a datum plane or focusing plane. These defocusings (in contrast to the instrumental defocusings associated with specific excitation of an objective lens) can be named as the habit defocusings. These defocusings are considered in this paper in the frameworks of the 2-D approximation with the help of intensity profiles, but results obtained and recommendations elaborated here are true for intensity distributions i.e., for 3-D situations.

Action of a probe on an object in the presence of habit defocusings is described by an action curve which is characterized by the expression [13, 14]:

$$I_{\Sigma} = \int_{X} \frac{J}{\sqrt{\pi}\sigma} \exp\left(-\frac{(x - x_c)^2}{\sigma^2} \right) \mathrm{d}x_c \tag{1}$$

Here, in the linear approximation,

$$\sigma = k\left(|z - f| \cdot \frac{R - r_f}{f} + r_f \right) \tag{2}$$

I_{Σ} is the total action of the probe at scanning, J is the total intensity of the probe, x_c is the coordinate of the centre of the probe, z is the distance from the point on the surface of the object to the output diaphragm of the objective lens, f is the focal length, $|z - f|$ is the distance from the point at the surface of the object to the focusing plane, therefore σ depends on an object height, r_f is the effective radius of the beam-section at the focusing (datum) plane, R is the radius of the exit aperture of the objective lens, r_f is the effective cutoff radius of the beam cross-section in the focusing plane, k is the coefficient depends on the effective cutoff radius, the region of integration X is determined by a lateral size of the object along the specified direction. In these formulas, $\sigma = \sigma_G / \sqrt{2}$ where σ_G is the root-mean-square deviation (the characteristic of the Gauss distribution) and the proportionality of σ to σ_G is the important property of the approach, since it allows using the software instruments, already created for modelling SEM images, also for processing of images obtained with the help of convergence beams.

The intensity distributions for images obtained in conditions of a 2nd convergence can be described as the sum of two components. The first component is a distribution that is independent of a convergence of the illuminating electron beam and, hence, does not reflect the shape of the object. The second component is determined by the changes in the sizes of the probe during its motion over the surface of the object, i.e., by the habit defocusing. Therefore, in order to determine the component

dependent on the habit defocusing, the component independent of the convergence of the illuminating electron beam should be eliminated from the total distribution. A curve arising in the result of the subtraction of action curves corresponding to probes with different convergences is referred subsequently as the differential curve. The differential curve is described by the expression:

$$I_{-} = \int_X \frac{J}{\sqrt{\pi}\sigma_2} \exp\left(-\frac{(x-x_c)^2}{\sigma_2^2}\right) dx_c - \int_X \frac{J}{\sqrt{\pi}\sigma_1} \exp\left(-\frac{(x-x_c)^2}{\sigma_1^2}\right) dx_c \quad (3)$$

where I_{-} is the total extent (intensity) of action due to the habit defocusing, and σ_1 and σ_2 correspond to 1st and 2nd convergences.

3. Experimental techniques to the habit determination.

3.1. Technique based on reconstruction a three-dimensional image in the real space.
If cross-sections of the illuminating beams with different convergences by certain plane are of identical in sizes so the Exp. (3) for a point of a differential curves at this plane converts to [13]:

$$\int_X \frac{J}{\sqrt{\pi}\sigma_2} \exp\left(-\frac{(x-x_c)^2}{\sigma_2^2}\right) dx_c - \int_X \frac{J}{\sqrt{\pi}\sigma_1} \exp\left(-\frac{(x-x_c)^2}{\sigma_1^2}\right) dx_c = 0 \quad (4)$$

Therefore effect of these beams on all points of this plane is also identical.

It is evidently on physical grounds, if two impacts are identical, so responses to these impacts are also identical, i.e., in line with Exp. (4), yields of recoil electrons are independent of convergences of the illuminating beams in all points of a focusing plane. If the 1st convergence is used, all points of an object are concurrently in-focus. Therefore if an intensity profile corresponding to the 1st convergence to lay over an intensity profile corresponding to the 2nd convergence, they intersect, to a first approximation, at a point where the focusing plane intersects the intensity profile conforming to the 2nd convergence. Consequently, if to focus the probe initially on the datum plane and thereupon to shift the focusing plane for known distance to a certain object cross-section so this procedure provides determining a distance between points of an intensity profile, lying in this cross-section, and the datum plane. Reiteration of this procedure allows to determine distances for many points of profile (including a height of an object summit) and to transform an intensity profile in the intensity space into a three-dimensional image in the real space (Fig.3). Overlapping of intensity profiles can be changed by profile subtraction and in this case, an extreme of the differential curve (maximum or minimum depending on what profile is the deduction) or a sign inversion of the differential curve can be observed.

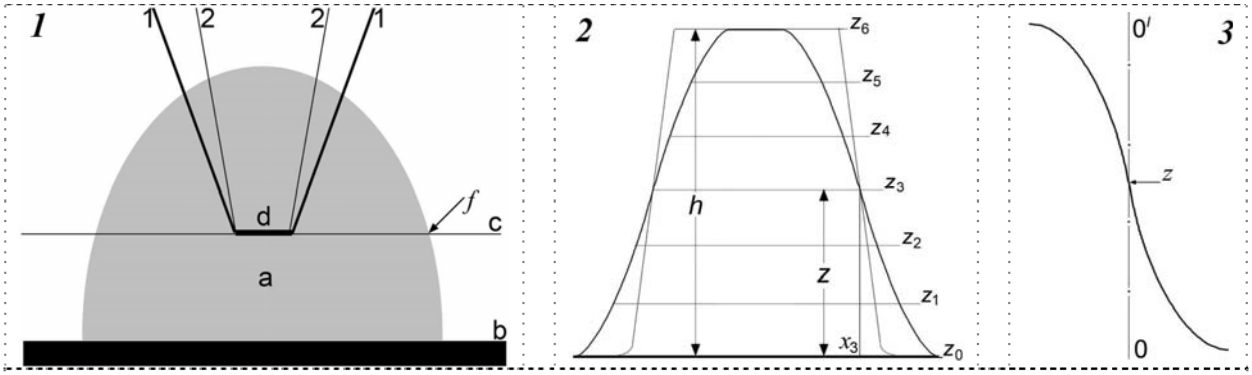

Figure 3. Illustrations to the method of obtainment of images in the real space. ***1*** – Diagram illustrating conditions of obtaining of contention profiles. 1, 2 are generatrixes of illuminating beams, "a" is an object, "b" is a substrate surface, "c" is the focusing plane, "d" is a cross-section of illuminating beams by the focusing plane, "*f*" is the point at an object surface, wherein impacts of illuminating beams are equal. ***2*** – Illustration to superposition of intensity profiles corresponding

different convergences for an object with a trapezoidal shape; a thin line profile corresponds to the 1st convergence; a heavy line profile conforms to the 2nd convergence. z_0 is the datum plane (a substrate surface); z_i are traces of focusing planes; z_3 is the focusing plane for a beam with 2nd convergence; z is a distance of the focusing plane from the datum plane; h is an object height; x_3 is an x-coordinate of the point z_3. **3** – Differential profile corresponding to Fig. 2; 00′ is the zero line; z is a point of a sign reversal of the profile.

3.2. Technique based on direct reconstruction of a habit.

Approach based on focusings upon object cross-sections is applicable only to objects which are of height exceeding 10 nm and, accordingly, provide sizeable habit defocusings. Problems of morphological identification of particles with sizes ≥ 10 nm can be solved on the base of another approach that can be named as the method of the direct habit reconstruction.

Two terms of Exp. 3 reflect identical dependences on the same variable and in the same interval; therefore Exp. 3 can be transformed as:

$$I_{-} = \frac{J}{\sqrt{\pi}} \int_{-\infty}^{\infty} \left[\frac{1}{\sigma_1} \exp\left(-\frac{(x-x_c)^2}{\sigma_1^2} \right) - \frac{1}{\sigma_2} \exp\left(-\frac{(x-x_c)^2}{\sigma_2^2} \right) \right] dx_c \qquad (5)$$

Let $|\sigma_2 - \sigma_1| \ll \sigma$, that allows realizing the linearization of the Exp (5) by means of the replacement of the difference of functions by the difference of arguments multiplied by the derivative. If σ_i to represent as $\sigma_i = \sigma_0 + \tau$ (where σ_0 is a size of the beam-section by a focusing plane and $\tau = k\{|z - f| \times (R - r_f)/f\}$ reflects σ changes due to the habit defocusing) and to take into account, that σ is equal to σ_0 over an extent of a profile for the 1st convergence, so the Exp. (5) can be put into the form:

$$I_{-} = \frac{J}{\sqrt{\pi}} \int_{-\infty}^{\infty} \frac{\tau}{\sigma_0^2} \left[1 - 2\frac{(x-x_c)^2}{\sigma_0^2} \right] \exp\left(-\frac{(x-x_c)^2}{\sigma_0^2} \right) dx_c \qquad (6)$$

Exp. (6) emphasizes one-to-one correspondence between habit defocusings and differential curves.

Differential curves differ fundamentally from intensity profiles, since they carry identified information (which misses for profiles) concerning all three dimensions. On the strength of Exp. (2) an electron distribution in a probe conforming to a beam with the 2nd convergence and its size differ from those of a beam with the 1st convergence and these differences increase with distance from the focusing plane (linearly for sizes and inversely quadratically for intensity distributions). Therefore calculations on the base of differential curves allow reconstructing a habit. In some cases, when $\sigma_0 \gg \tau$, habits can be built in accordance with the Eq. (6) on the base of differential curves by means of the reciprocal integral transformation or matrix inversion, but in the majority instances, the condition $\sigma_0 \gg \tau$ is difficult implemented and reconstruction must realized on the base of these curves and software resulting from Exp. (5).

Besides, software must take into account that electrons registered in SEM correspond not to electrons of illuminating beams but to recoil electrons, and, accordingly, obtained curves are not the differential curves but curves of differences of intensity profiles. Therefore soft must include operations reflecting links of regularities of the yield of recoil electrons and, correspondingly, allowing transforming an experimental profile differences into the differential curves. These operations must take into consideration, that: firstly, intensity of recoil electrons depends on a tilting of a facet about a microscope axis; secondly, if a probe conforming to the 2nd convergence is located wholly on a plane facet, so the yield of recoil electrons is equal to their yield for the 1st convergence, i.e., this portion of profile difference must be of a zero level; thirdly, if a probe comes nearer to a line of an intersection of facets at a distance less then the free path of electron of the given energy, so recoil electrons can be emitted through two surfaces and an intensity maximum arises, fourthly, if a probe is distributed between surfaces with different yields of recoil electrons, so their yield is a sum of

yields emitted by each facet; fifthly, the antecedent rule is true also for probes distributed between an object and substrate. Listed rules cannot restrict the applicability of the described approach since each change of conditions of the yield of recoil electrons reflects on intensity profiles and a curves corresponding to their differences and these notches must be included in the software. At that, the information associated with differences of notch positions at intensity profiles, corresponding to different convergences, and a distance between notches at a curve, reflecting their difference, is the major factor allowing correct reconstruction of the differential curve.

Identification of minute particles is hampered since very small habit defocusings are associated with these objects. This impediment can be surmounted with 2 variants of a special method of obtaining a differential curve. In the framework of this method, 3 planes (central and 2 lateral) are used in SEM (Fig. 4). In the first variant, two defocused images are formed by means of alternate coincidences of the focusing planes with two planes that are equidistant with respect to the plane of the object localization (Fig. 4-a). In the second variant, the focusing plane is brought into coincidence with the central plane and the object is coincided with two planes that are equidistant with respect to the central plane (Fig.4-b). It should be shown that the equidistance is optical one; i.e., the cross sections of the illuminating beam by two profile planes are identical to each other upon focusing onto the central plane, but, upon focusing onto the lateral planes, there arise equal cross sections in the central plane irrespective of the plane onto which the beam is focused. Since these two images correspond to the same datum plane, the subtraction of one of the relevant intensity distributions from the other distribution also gives rise to a differential profile that depends uniquely only on the habit of the object.

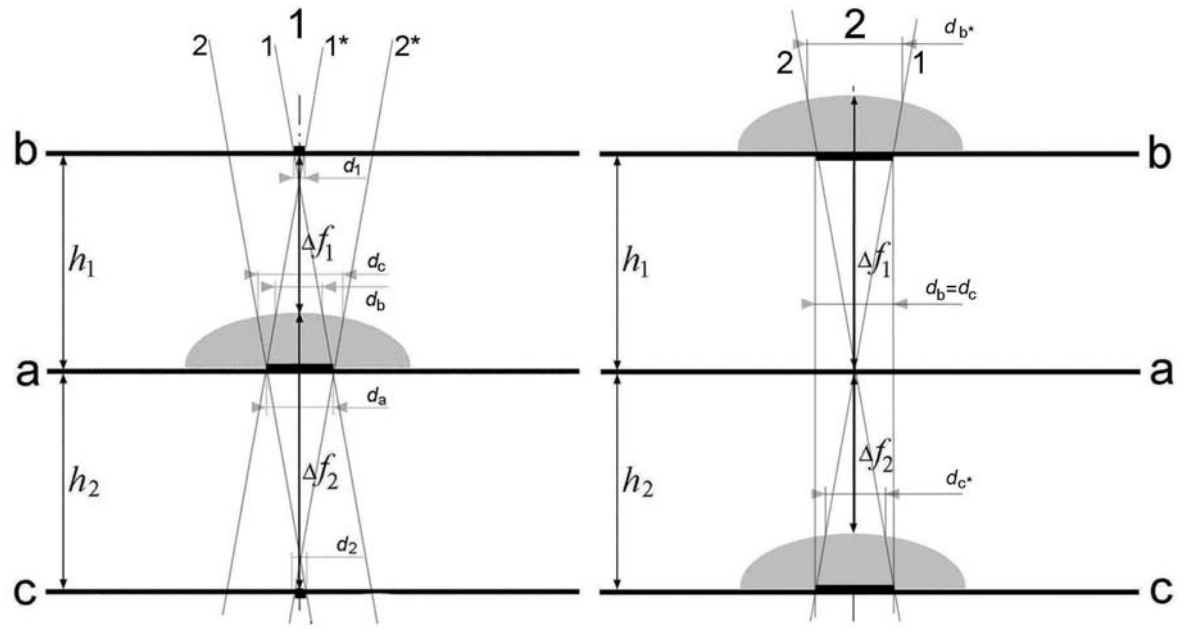

Figure 6. Schemes illustrating the specific features of the implementation of the technique: (**1**) the scheme reflecting the specific features of the image formation in the case where the beam is focused onto two equidistant planes (**b** and **c**) and the datum plane is brought into coincidence with the central plane (**a**); (**2**) the scheme reflecting the specific features of the image formation in the case where the datum plane lies in equidistant planes (**b** and **c**) and the beam is focused onto the central plane (**a**). In both schemes, h_1 and h_2 are identical distances due to changes in the sizes of the cross sections of the illuminating beam. Designations in scheme (**1**): 1 and 1* are the generatrices of the cone of rays in focusing onto the **b** plane; 2 and 2* are the generatrices of the cone of rays in focusing onto the **c**

plane; d_1 is the size of the cross section of the beam by the **b** plane and d_2 is the size of the cross section of the beam by the **c** plane ($d_1 = d_2$); d_a is the size of the cross section of the beam by the **a** plane, which is identical for both defocusings; Δf_1 is the distance from the top point of the object to the **b** plane and Δf_2 is the distance from the top point of the object to the **c** plane ($\Delta f_1 < \Delta f_2$); d_b is the probe size in focusing onto the **b** plane and d_c is the probe size in focusing onto the **c** plane ($d_b < d_c$). Designations in scheme (**2**): 1 and 2 are the generatrices of the cone of rays in focusing onto the **a** plane; Δf_1 is the distance between the top point of the object with the datum plane in the **b** plane and the focusing plane **a;** Δf_2 is the distance between the top point of the object with the datum plane in the **c** plane and the focusing plane **a** ($\Delta f_1 > \Delta f_2$); d_b and d_c are the sizes of the cross sections of the beam by the **b** and **c** planes, ($d_b = d_c$); and d_{b*} and d_{c*} are the probe sizes in the case where the zero-height planes of the object lie in the **b** and **c** planes, respectively ($d_{b*} > d_{c*}$).

In the both variants of the technique, when images corresponding to different defocusings for each point on the surface, it can be write $|\tau_1| = |\tau_2|$, but the quantities τ_1 and τ_2 have different signs depending on the defocusing sign. As a result, expression (3) can be represented in the form:

$$I_{-} = \frac{J}{\sqrt{\pi}} \int_{-\infty}^{\infty} \frac{2\tau}{\sigma_0^2} \left[1 - 2\frac{(x - x_c)^2}{\sigma_0^2} \right] \exp\left(-\frac{(x - x_c)^2}{\sigma_0^2} \right) dx_c \qquad (6)$$

Consequently, the technique provides obtaining a differential curve which, at that, displays twofold increasing sensitivity to the habit defocusings. The latest circumstance allows, firstly, to use this technique for investigations of the minute particles which give rise to negligible habit defocusings, and, secondly, to minimize a necessary value of convergence that simplifies the problem of the correction of the spherical aberrations and provides more precise execution of the condition $\tau \to 0$; that is especially important when the minute particles are studied.

4. Conclusion.

Enlargement of a convergence of illuminating beam enlarges dramatically spreading a probe in the result of the spherical aberration. Possibilities of limitation of the spherical aberration effect (including aberration associated with large angles of the beam convergence) have been solved in [15]. For the implementation of the method, it is necessary to vary the convergence of the illuminating electron beam at precisely specified values. The problem of variation in the angles of convergence is solved by using a two-lens condenser and sets of condenser and objective diaphragms in [16].

The key problem governing the implementation of the proposed approach is to bring the datum plane into coincidence with the focusing plane. For nanodimensional objects, these planes must be brought into coincidence with angstrom accuracy. The coincidence of the planes with this accuracy (especially the planes with the a priori unknown relief) cannot be achieved in frameworks of using SEM techniques (even with images arising in conditions of large convergences of illuminating beams). Therefore microscope must have the “limit stop” which breaks off movement of a microscopic stage when the datum plane coincides with the focusing plane. Controllers of the type used in SPM [17] provide solution of this problem.

Both the suggested techniques (the three-dimensional image and the direct habit reconstruction) cannot provide obtaining an exact habit on the strength of specific peculiarities of SEM images if even all shown above technical problems are solved. However their results reflect sizes and a shape of an object and, consequently, can be used as virtual prototypes of an object, and, at that, a further correction of object parameters can be carried out with the help of the familiar procedure involving receipt of the prototype image in conditions corresponding to the conditions of obtaining the original object image and subsequent fitting of this prototype image to the experimental object image by means of variations of prototype shape and sizes. Different software products intended for the computation of virtual images (e.g. Joy’s PC Monte Carlo programs, Casino Monte Carlo Program, SEMLP, etc) can

be used for this aim. Joint use of the suggested methods and developed computer methods of SEM image processing provides the true habit determination.

It must be emphasized that although approaches grounded on the transformation of intensity distributions into three-dimensional images or obtaining a differential profiles are very time consuming, they can be recommended also for outgoing control in nanotechnologies, since the shown shortcoming becomes unobtrusive in this case. Habit identification is obligatory process only on the stage of designing a technique for a new objects or new technologies, but current control can be carried out only by scanning of massifs, obtaining their images, and the classification of these images on the base of found dependences between object shapes and image characteristics. Therefore the suggested methods can be suggested also as the constituent part of the outgoing inspection.

Although the process of determination of dependences between characteristics of SEM images and structural-morphological characteristics of particles is carries out only during the stage of development of technology of a given type of produce, it remains the key phase of the suggested approach to all outgoing control, since only this phase allows ascertaining potential risky kinds of particles. Therefore this phase demands a thorough inspection of even single images if the slightest doubts are cast upon their nature. The phase of obtaining of images of large massifs of particles is principal in the frameworks of the given approach, and not only because that it is the single inspection process of a production stage but also since it is process allowing exposing objects demanding further control. Therefore this process demands rigorous identity of conditions of image formations of a massif as a whole.

Acknowledgments. The authors would like to thank the staff of the Abdominal Department of the Moscow P.A.Herzen Oncology Research Institute whose efforts have made possible the appearance of this publication.

References

[1] Nanotoxicology. Characterization, Dosing and Health Effects. Eds. Montairo-Riviere N., Tran L.C. // Informa Healthcare USA Inc. 2007. 450 P.

[2] S. Zuin, G. Pojano, A. Marcomini. Effect-Oriented Physicochemical Characterization of nanomaterials.19 – 57. // Nanotoxicology. Characterization, Dosing and Health Effects. Eds. Montairo-Riviere N., Tran L.C. // Informa Healthcare USA Inc. 2007. PP. 19-58.

[3] A.S. Barnard A special issue on theory and simulation of nanomorphology. // J. of Computational and Theoretical Nanoscience. 2007. V. 4. No 2. PP. i-ii

[4] G. Guisbiers, G. Abulimu, F. Clement, M. Wautelet. Effects of Shape on the Phase Stability of Nanoparticles. // J. of Computational and Theoretical Nanoscience. 2007. V. 4, No 2, PP. 309-315.

[5] S.K. Maksimov; K.S. Maksimov. Controlling the surface functionality of nanomaterials. Nanotechnologies in Russia, 2009. V. 4, No 3–4, PP.188–200.

[6] S.K. Maksimov, K.S. Maksimov.. Principles of nanomaterial control for development of safety standards as illustrated by establishing of Laws of Nanostructuring in $Ca_yLa_{1-y}F_{3-y}$ and $La_xCa_{1-x}F_{2+x}$ solid solution. Technical Physics Letters, 2009, V. 35, No 3. PP. 224 – 227.

[7] Linglan Ma, Jinfang Zhao, Jue Wang, et al. The Acute Liver Injury in Mice Caused by Nano-Anatase TiO_2. // Nanoscale Res Lett. 2009, No 4, PP. 1275–1285.

[8] R. Ravichandran. Physico-chemical evaluation of gymnemic acids nanocrystals. Int. J. Nanoparticles, 2010, No 3, PP. 280-296.

[9] Nanocharacterization. Eds. Hutchison J., Kirkland A. // RSC Publishing, 2007, xii + 304 P.

[10] Fan Yang, Fashui Hong, Wenjuan You, et al. Influences of Nano-anatase TiO_2 on the Nitrogen Metabolism of Growing Spinach. // Biological Trace Element Research, 2006, V. 110, No 2, PP. 179–190.

[11] S.K. Maksimov, K.S. Maksimov. // Concept of safety standard and outgoing inspection in

technologies of nano-particles. // Nanotechnics, 2009, No 18, PP. 5 – 12. (in Russian).
[12] D.E. Newbury, D.C.Joy, P. Echin, C.E. Fiory, J.I.Goldstein. Advanced Scanning Electron Microscopy and X-Ray Microanalysis. // Plenum Press. N.Y., L. 2003, 634 P.
[13] S.K. Maksimov, K.S. Maksimov. New approach in metrology for nanotechnologies. // Technical Physics Letters, 2010, Vol. 35, No. 10, PP. 938–941.
[14] K. S. Maksimov. Systematic Features of Defocused Images in Scanning Electron Microscopy and Nanoscale Size Measurements. // Semiconductors, 2009, Vol. 43, No. 13, PP. 1725–1727.
[15] Kawasaki, T. Yoshida, Y. Ose, H. Todokoro. // Electron beam apparatus with aberration corrector. // USPat. 7,199,365. 2007.
[16] H. Kitsuki; K. Aoki; M. Sato. Scanning electron microscope. // USPat. 7,442,929. 2008.
[17] B. Bhushan, O. Marti. Scanning Probe Microscopy – Principle of Operation. Instrumentation and Probes. (2007). Springer Handbook of Nanotechnology, 2nd ed. (Ed. by Bharat Bhushan), PP. 239–278.